Published in Journal of Lightwave Technology 15, issue 4, 663-670, 1997
which should be used for any reference to this work

Optical Displacement Measurement with GaAs/AlGaAs-Based Monolithically Integrated Michelson Interferometers

Daniel Hofstetter, Hans P. Zappe, and René Dändliker

***Abstract*—Two monolithically integrated optical displacement sensors fabricated in the GaAs/AlGaAs material system are reported. These single-chip microsystems are configured as Michelson interferometers and comprise a distributed Bragg reflector (DBR) laser, photodetectors, phase shifters, and waveguide couplers. While the use of a single Michelson interferometer allows measurement of displacement magnitude only, a double Michelson interferometer with two interferometer signals in phase quadrature also permits determination of movement direction. In addition, through the use of two 90° phase-shifted interferometer signals in the latter device, a phase interpolation of $2\pi/20$ is possible, leading to a displacement resolution in the range of 20 nm. The integration of these complex optical functions could be realized with a relatively simple fabrication process.**

***Index Terms*—Distributed Bragg reflector lasers, optical device fabrication, optical distance measurement, optical interferometry.**

I. Introduction

THE first measurements using the interferometer which bears his name were carried out by Michelson in 1881 [1]–[3]. This historical experiment proved that the speed of light was not influenced by the motion of the earth relative to a hypothetical ether. The same experimental setup was subsequently used for spectroscopic and displacement measurements. In that age, gas vapor discharges were the only available spectrally pure light sources, such that displacement measurements were limited to distances of about 1 m due to the limited coherence length of the source. Using highly coherent laser light, interferometric displacement measurement is possible at distances exceeding 100 m [4] and represents an important research and industrial tool.

Using the technology of integrated optics, light is propagated in waveguides instead of free space, implying that extremely small optical circuits can be fabricated. Integrated optical sensors using waveguides are thus very compact and physically robust and may easily be fabricated by mass-production techniques [5]. For these reasons, integrated optical Michelson interferometers have become very attractive for optical displacement measurement, both in the laboratory and for applications in the field.

We present in this paper the design, fabrication technology and characterization of III–V semiconductor-based, monolithically integrated displacement sensors. These fully integrated measurement microsystems include all active interferometer components on a single semiconductor chip. Following a brief survey of previous work in this field, we will present the required processes for the fabrication of a semiconductor-based interferometer, discuss distributed Bragg reflector (DBR) lasers as light sources and selective bandgap shifting for on-chip transparency. We will then present the performance characteristics of both the single Michelson interferometer (SMI) [6] and the double Michelson interferometer (DMI) with two 90° phase-shifted reference beams [7] and conclude with a comparison of these structures and existing displacement sensors.

II. Summary of IO Displacement Sensors

Due to the attractive features of an integrated optical (IO) approach, numerous workers have developed Michelson interferometer-based displacement sensors using various technologies. One of these approaches has been described by Ulbers [8] and was commercially available for some time (Hommelwerke Sensor GmbH) [9]. This device consisted of a Michelson interferometer on a silicon chip where waveguiding was by planar waveguides. An external gradient index (GRIN) lens was used for the collimation of the measurement beam; in addition, an external diode laser and photodetectors were required for stimulation and signal measurement.

The IO Michelson interferometer fabricated by Jestel [10] used ion-exchange stripe waveguides on a glass substrate, thermo-optic phase shifters to define the relative phase shift between the two reference arms and directional couplers to divide the incoming light into reference and sensing beam. This device consisted of two combined Michelson interferometers (often referred to as a double Michelson interferometer) and allowed direction determination of the movable object. It also required an external diode laser and external photodetectors, plus one externally mounted beam-shaping element.

D. Hofstetter was with the Paul Scherrer Institute, 8048 Zurich, Switzerland. He is now with the Xerox Palo Alto Research Center, Palo Alto, CA 94304 USA.

H. P. Zappe is with the Paul Scherrer Institute, Badenerstrasse 569, 8048 Zurich, Switzerland.

R. Dändliker is with the Institute of Microtechnology, University of Neuchâtel, 2000 Neuchâtel, Switzerland.

The measurement of displacement is also possible with Mach–Zehnder type interferometers; Voirin [11] reported a Mach–Zehnder interferometer for this application. This sensor was fabricated in glass with ion-exchange stripe waveguides and wavelength-stabilized to within 10^{-6}. The usual external elements, namely laser, detectors and GRIN lens, were again necessary to operate the interferometer.

Recently, Suhara [12] published a monolithically IO position sensor. This III–V-semiconductor-based device was configured as a double Michelson interferometer and consisted of a DFB laser, planar waveguides, and grating couplers but without a phase shift between the two reference beams. The grating coupler served as beam splitter and also as collimation lens for the measurement beam. A similar device with two phase-shifted interference signals but without an integrated DFB laser was demonstrated in 1989 [13].

III. III–V Processing

Monolithically integrated optical circuits, fabricated in a III–V semiconductor system, have been extensively developed for telecommunication applications; the material systems used have been chosen for their suitability for the fabrication of lasers at the required wavelengths. Integration of the components necessary for an optical circuit requires the ability to fabricate an integratable laser, a means to selectively define transparency across the chip, and techniques for achieving electrical and optical isolation between devices. We will provide here an overview of the more salient aspects of the fabrication processes required for the interferometers.

A single layer structure was used for all required devices and was grown by metal-organic vapor phase epitaxy on a GaAs substrate (n-doped 10^{18} cm^{-3} Si). An undoped 165-nm-thick $Al_{0.3}Ga_{0.7}As$ waveguide core containing a single GaAs quantum well (7 nm) was sandwiched between a 1.1-μm-thick $Al_{0.8}Ga_{0.2}As$ lower cladding layer (n-doped 1.5×10^{18} cm^{-3} Si) and an 0.85-μm-thick $Al_{0.8}Ga_{0.2}As$ upper cladding layer (p-doped 10^{18} cm^{-3} Mg). A 160-nm-thick highly p-doped (5×10^{18} cm^{-3} Zn) GaAs cap layer completed the structure. As we will discuss below, a postgrowth bandgap shifting technique was used to selectively define transparency across the wafer, such that only a single epitaxy step was required.

Using a standard dry etch chemistry, 3-μm-wide ridge waveguides were etched to a depth of 100 nm above the waveguide core; this was followed by the dry etch of a 500-nm-deep optical isolation trench between laser and detectors, which was subsequently filled with p-metal layers. Passivation and electrical isolation of the ridge sidewalls was achieved through a 250 nm thick PECVD-grown Si_3N_4-layer. Proton implantation ($H^+, 4 \times 10^{15}$ cm^{-2}, 40/70/100 keV) and a cap etch, outside all contact areas, were used to generate a high electrical resistance between laser and photodetectors (>10 GΩ). After a contact hole etch on top of the ridges, standard p- and n-metal layers were evaporated.

Fabrication of the DBR grating involved the dry etch of a grating recess to a depth of about 230 nm above the core. The third order grating was then defined by holographic exposure and subsequent dry etching. Cleaving of the bars to the desired length and evaporation of suitable facet coatings completed the processing. On the left laser facet, we used a high-reflection (HR) coating in order to reduce the laser threshold current; and on the right interferometer facet, an antireflection (AR) coating was evaporated to improve interferometer signal contrast.

A. Selective Bandgap Shifting

The combination of lasers and transparent waveguides requires the definition of sections with different bandgap energies on the same substrate. The methods to solve this problem can be divided into growth- and intermixing approaches. The most popular among the growth methods are selective area growth [14]–[16] and etch and epitaxial regrowth on a nonplanar patterned substrate [17], [18]. The first allows the *simultaneous* epitaxy using different growth rates, and, therefore, the growth of quantum wells with different thicknesses. In contrast to this, the second uses a *subsequent* growth of material with different quantum-well (QW) thicknesses. Other possibilities are selective partial intermixing of the QW using impurities [19], [20] or vacancies [21]. The primary advantage of the intermixing methods is that they require no additional regrowth, whereas the high temperature rapid thermal annealing (RTA) step necessary can lead to dopant migration. We employed an impurity-free intermixing approach, vacancy-enhanced disordering (VED), for the definition of transparent regions.

The VED technique required that the sample be completely covered with a single layer of either e-beam evaporated SiO_2 or thermally evaporated SrF_2. During RTA at 960 °C for 30 s, group-III-vacancies are generated under the SiO_2-cap but not under the SrF_2-cap. Under SiO_2, the vacancies promote intermixing of the Ga in the initially pure GaAs QW with Al of the adjacent $Al_{0.3}Ga_{0.7}As$ core, thereby increasing the Al-content and the energy bandgap of the QW. The final effect is an anneal temperature-dependent blue-shift of the photoluminescence (PL) spectrum. Fig. 1 shows the achieved blue-shifts as a function of temperature and anneal time. After an RTA of 30, 60, and 90 s duration, and at temperatures between 910–960°C, we measured blue-shifts of 5–68 nm under the SiO_2-cap and less than 10 nm under the SrF_2-cap. Both dielectrics are stripped by wet or dry etchants after the anneal step.

This means to selectively promote a blue-shift in the absorption wavelength can then easily be used to define transparent regions in a quantum-well, waveguide-based optical circuit; for the applications discussed below, the passive waveguides and couplers were fabricated in regions covered with SiO_2 during anneal, whereas the lasers and photodetectors were defined in the unshifted regions defined by SrF_2.

B. Bandgap-Shifted Fabry–Pérot Lasers

In order to demonstrate the good laser quality of material subject to a VED anneal, we fabricated Fabry–Pérot lasers in both the shifted and the unshifted regions of annealed material, as well as in as-grown material in a process described previously [22]. The lasers were 500 μm long with a ridge width of 4 μm and were tested in bar form under

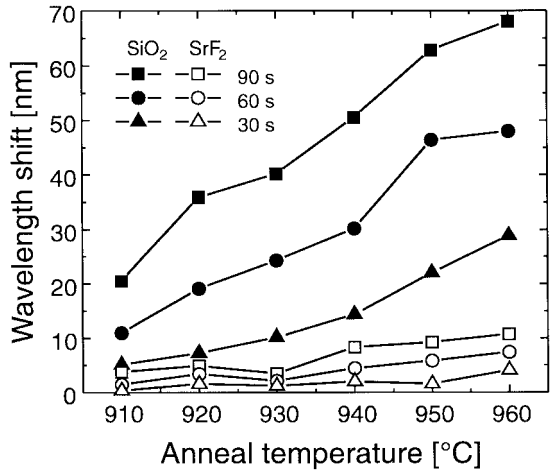

Fig. 1. Photoluminescence wavelength shift of SiO_2-capped and SrF_2-capped material after vacancy-enhanced disordering at different anneal temperatures and anneal times. Excitation of the photoluminescence was accomplished with an argon-ion laser ($\Lambda = 488$ nm, $P = 10$ mW) and measured at room temperature.

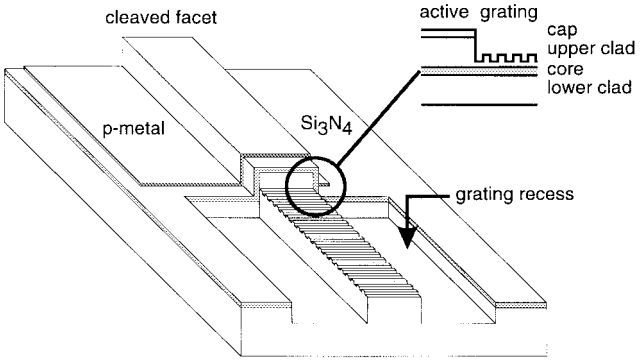

Fig. 2. Schematic picture of a single-growth-step DBR laser with a holographically-defined, grating fabricated in a grating recess.

CW conditions at room temperature. The spectra of representative as-grown, SrF_2-, and SiO_2-capped devices showed laser emission at wavelengths of 826, 823, and 805 nm, respectively; thus the VED-induced wavelength shifts were 3 and 21 nm.

The as-grown laser had a threshold current of 12 mA ($J_{th} = 600\,\text{A/cm}^2$) and a slope efficiency of 0.52 W/A. A maximum output power of 14 mW at $I = 4\times I_{th}$ was achieved. In comparison, the P–I-curve of the SiO_2-capped laser had a lower threshold current of 10 mA ($J_{th} = 500\,\text{A/cm}^2$) while the SrF_2-capped device had a somewhat higher threshold current of 14 mA ($J_{th} = 700$ A/cm^2). The slope efficiencies of the SiO_2-capped laser (0.42 W/A) and the SrF_2-capped laser (0.36 W/A) were lower than that of the as-grown laser. The higher threshold current and lower slope efficiency of the SrF_2-capped laser were probably caused by repeated plasma exposure of its contact region during SiO_2 removal, SiO_2 patterning and Si_3N_4 patterning.

C. DBR Laser

Numerous approaches have been developed for the integration of a laser with an optical circuit; these include evanescent coupling between waveguides and emitting regions (requiring an additional impedance matching layer and regrowth) [23], [24], butt coupling between laser and photodetector (needing a mirror dry etch technique) [25] or the use of surface emitting lasers and photodiodes (requiring high-quality dry-etched mirrors) [26]. For the present work, the use of a simplified, single-growth-step, two section DBR laser, described previously [27], [28], represents an attractive solution with respect to both process compatibility and feedback stability for an integrated interferometer.

The pumped section of the laser was fabricated in an area of the chip not subject to a bandgap shift during VED, while the Bragg reflector was etched into the shifted, thus transparent, region. The use of a so-called grating recess (see Fig. 2) allowed accurate vertical placement of the grating [28]; this recess was dry etched to within 150 nm of the active region, leaving an accurately defined layer for the Bragg reflector. The holographically defined third order grating had a period of 375 nm, 1:1 line-to-space ratio and 100 nm depth. The 50 nm thick buffer layer between grating and waveguide core determined the coupling coefficient, approximately 100 cm^{-1}.

Performance evaluation of discrete DBR lasers was carried out CW at room temperature. As seen in the inset to Fig. 3, maximum output power was 5 mW from the cleaved facet, threshold current was 26 mA ($J_{th} = 1.3$ kA/cm^2) and slope efficiency was on the order of 0.21 W/A. The latter value could be further improved by ensuring a closer wavelength match between the Bragg peak of the grating (820 nm) and the semiconductor gain peak (825 nm). The laser spectrum, as shown in Fig. 3, was single longitudinal mode with a primary emission peak at $\lambda = 820$ nm and had a side-mode suppression ratio (SMSR) of 27 dB. High-resolution spectral measurements and detailed near-field studies indicated that the laser operated with a single transverse mode. Self-heterodyne measurements of the laser spectrum gave a spectral linewidth of 500 kHz.

From the Fabry–Pérot mode spacing of 0.16 nm, we could calculate the effective cavity length to be about 630 μm implying an active grating length of approximately 130 μm. The primary emission peak could be continuously temperature-tuned between 15–35 °C, leading to a temperature tuning coefficient of 0.06 nm/°C.

D. Integration: Laser, Waveguide, and Photodetector

To test the suitability of these DBR lasers and the VED technique for bandgap shifting described above, a simple optical circuit consisting of 500 μm long pumped laser sections, 130 μm long nonabsorbing DBR reflectors, 570 μm long transparent waveguides, and 500 μm long absorbing photodiodes was fabricated. The entire chip, 1700 μm long, was traversed by a single 4 μm wide waveguide.

As shown in Fig. 4, we simultaneously measured the cleaved facet output power with an external photodetector and the output power from the grating side of the laser with the integrated photodetector; for current values up to 35 mA, the two curves follow each other closely. Above this current level, the integrated photodetector seems to saturate, likely because no reverse bias voltage was applied. This operating

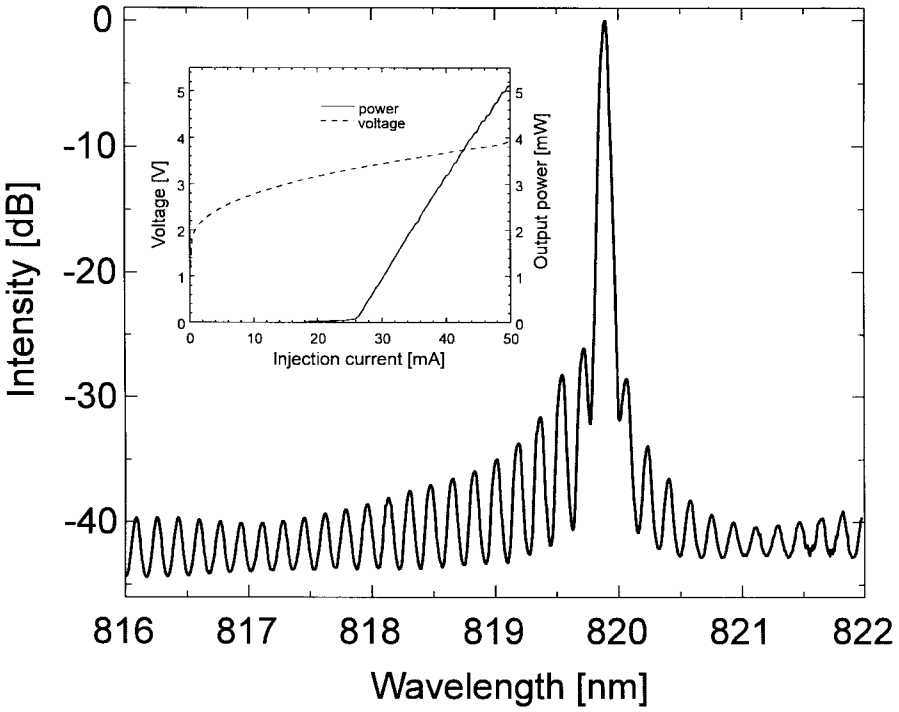

Fig. 3. Optical spectrum of a DBR laser with a 500-μm-long pumped and a 130-μm-long grating section driven at $2.3 \times I_{th}$. The inset shows the I–V- and the P–I-curve.

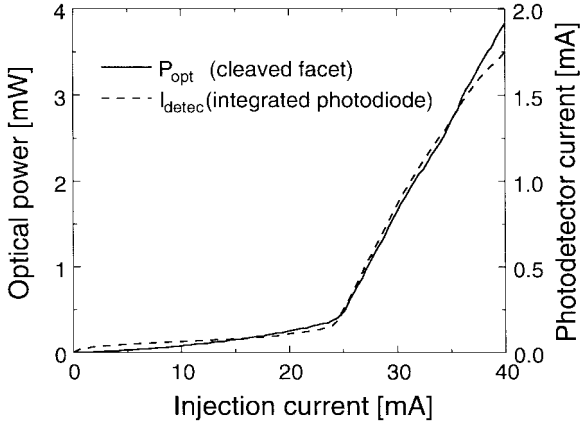

Fig. 4. Cleaved facet optical output power and photodetector current versus laser injection current of a DBR laser monolithically integrated with a transparent waveguide and an absorbing photodetector.

condition was chosen because the resistance parallel to the reverse biased photodiode is about 5 kΩ and thus leakage currents were relatively high.

The wavelength-shifted waveguides had optical losses comparable to as-grown transparent waveguides and were on the order of 1.5 dB for the short lengths (0.57 mm) employed. Photodiodes of this design typically have a high responsivity (>0.6 A/W), implying >90% quantum efficiency. If we assume that the laser output from the grating side (with reflectivity 30–40%) and the cleaved facet side (reflectivity 31%) are roughly equal, we can determine a total conversion efficiency of laser output into detector current of 0.47 A/W; no obvious performance differences between annealed and nonannealed photodetectors were noted.

IV. Interferometer Design and Characterization

The optical circuits we describe in this paper were configured either as single Michelson interferometers (SMI), or as double Michelson interferometers (DMI); both of them are shown schematically in Fig. 5(a) and (b). The SMI devices included a DBR laser, a photodetector, and waveguides forming a directional coupler, while the DMI's consisted of one DBR laser, two photodetectors, two Y-couplers, two directional couplers, and two phase shifters. The ridge width of the waveguides was 3 μm and all curve radii were 500 μm. The passive waveguides were fabricated in the areas with intermixed quantum wells and had, because of the relatively small bandgap difference of 45 meV between intermixed and nonintermixed sections, an absorption loss of 35–45 dB/cm. Since the total waveguide length did not exceed 3 mm, this relatively high absorption loss was not overly detrimental for interferometer performance. The total chip lengths were 1.95 mm for SMI's and 2.6 mm for DMI's.

Both the pumped laser section and photodetectors were fabricated in the nonintermixed, and thus absorbing, areas of the chip and had a length of 500 μm each. The length of the nonabsorbing DBR grating section was 200 μm; here, we used a third order grating with a period of 380 nm, a depth of 160 nm and 1:1 line-to-space ratio. A 70 nm thin buffer layer between the bottom of the grating and the waveguide core resulted in a calculated grating coupling coefficient of 100 cm^{-1}; this gave the desired grating reflection coefficient of about 95%. The left cleaved facet of the interferometer served as the second laser mirror.

These interferometer chips were tested in bar form and were temperature-stabilized to within $\pm$50 mK using a thermo-

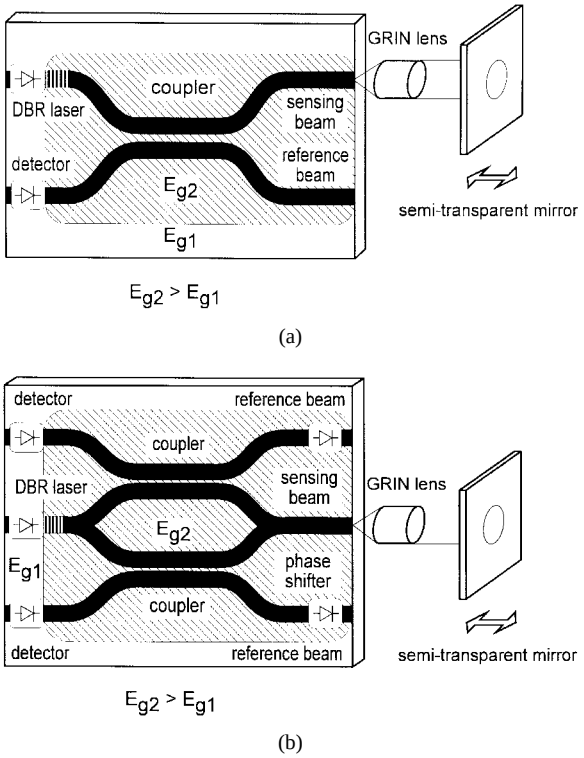

Fig. 5. (a) Schematic representation of a single Michelson interferometer for optical displacement measurement. (b) Schematic representation of a double Michelson interferometer for optical displacement measurement with direction determination.

electric cooler. The measurement beam, collimated by an external GRIN lens (pitch = 0.23), was directed onto a semi-transparent, 67% reflecting mirror through which the reflected beam position could be observed by a CCD camera. Observation was necessary to adjust the beam properly into autocollimation. By using a pitch of 0.23 instead of 0.25, we could prevent physical contact of the GRIN lens with the cleaved interferometer facet, reducing the probability of facet damage. The semi-transparent mirror was fixed to a piezo-driven, gimbal-mounted holder with which the measurement distance could be varied between 3–45 cm. Tilt control of this mirror was performed by piezo-actuators, resulting in a tilt accuracy of 0.33 μrad/V in the horizontal and of 0.67 μrad/V in the vertical direction. With this arrangement, we were able to produce either a 20 μm unidirectional movement, or a movement with periodically ($T = 60$ s) changing direction. The unidirectional movement was used to test the SMI's and led to 49 interference fringes, each of them corresponding to a mirror movement of 410 nm (see Fig. 6). The displacement with periodical direction changes every 2 μm was used to measure the characteristics of a DMI.

V. SMI Performance

The photodetector of the SMI was reverse biased at -5 V and had a leakage dark current of 500 pA; responsivity of such detectors is typically 0.6 A/W. The electrical resistance between the laser diode and the adjacent photodiode was

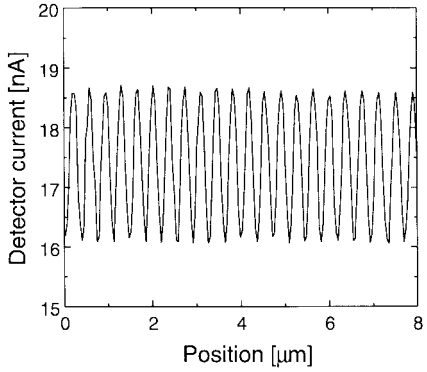

Fig. 6. Interferogram for 3-cm mirror distance and 95% mirror reflectance as measured by integrated photodetector using a SMI.

measured to be on the order of 10 GΩ and the optical output power from the interferometer was estimated to be about 2 μW. The measured interference signal is shown in Fig. 6; it exhibited a good temporal stability but was very sensitive to vibration of the external components. Displacements of a quarter of a fringe, or approximately 100 nm, were resolvable. With this single Michelson interferometer configuration, no determination of a change in movement direction is possible.

A large constant offset in the photodiode current, dominated by optical crosstalk between laser and photodiode, was seen. The interferometer signal as a function of the external phase ϕ, defined by

$$I(\phi) = I_{\text{cross}} + \frac{I_0}{2}\,(1 + V \cdot \cos\,\phi)$$

includes a constant offset in the detector current signal, I_{cross}, due to optical crosstalk between laser and detector, as well as a constant component $I_0/2$ due to visibility $V = (I_{\max} - I_{\min})/(I_{\max} + I_{\min})$ less than unity. This crosstalk current was reduced, but not completely eliminated, by the isolation trench between laser and photodiode. To evaluate this offset current, we removed the external optics and measured the signal magnitude. Since we know the reflectivity of the AR-coated facet ($\sim$2%), we were able to estimate a value of 15.8 nA for the crosstalk current from this measurement. This value agreed well with a more comprehensive measurement involving the use of five different external mirrors with differing reflectivities. Subtracting the crosstalk current from the signal values shown in Fig. 6 results in a considerably improved contrast ($V = 0.8$ instead of $V = 0.1$).

A plot of the corrected signal contrast (after subtraction of the crosstalk current) as a function of mirror distance is shown in Fig. 7. The Fourier-transformation of this autocorrelation function allows the estimation of the DBR laser linewidth; we calculated a value of 500 MHz, which is a factor of 10^3 larger than the value obtained with a discrete DBR laser. An investigation of the laser spectrum using a scanning Fabry–Pérot resonator exhibited an irregularly flickering spectrum with approximately the linewidth calculated above, and not the expected broadened Lorentzian-shaped laser

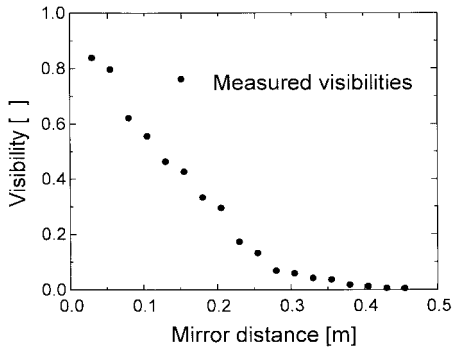

Fig. 7. Signal contrast as a function of mirror distance using a 67% reflecting mirror for the SMI.

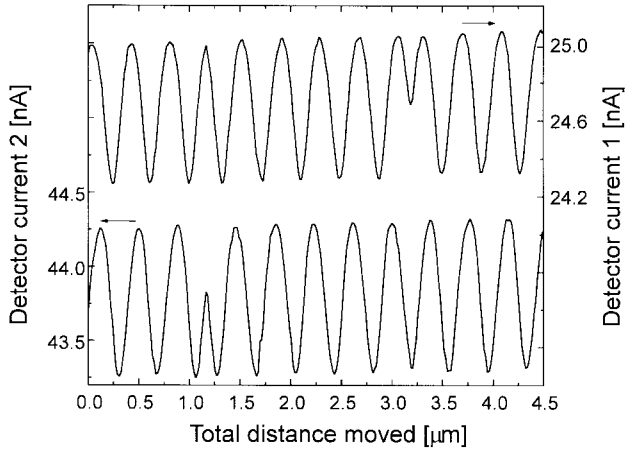

Fig. 8. The two detector currents of the double Michelson interferometer for 3.5 cm mirror distance and 67% mirror reflectance showing the two interference signals. Direction changes occurred at 1.2 μm and at 3.2 μm.

line. These observations indicate clearly that the laser sees numerous external cavities caused by facet reflections and tries to optimize their phase conditions. The short coherence length of the integrated DBR lasers therefore provides a fundamental system limitation; current work is focusing on the improvement of integrated laser linewidth.

VI. DMI Performance

The DMI's were characterized with the same setup as described above; the application of electrical bias to the phase shifters in the two reference arms allowed determination of changes in movement direction in addition to the magnitude of displacement. The DBR lasers operated at a current level of 60 mA and a reverse voltage of -12 V was applied to the photodetectors. The length of the phase shifters was 340 μm which gave a one-pass phase shift of $\pi/16$ when driven at -12 V bias voltage. Fig. 8 presents the result of an interferometric measurement with a DMI at a mirror distance of 3.5 cm.

Two changes of movement direction are clearly visible in the figure: one at 1.2 μm and another at 3.2 μm. Again, one interference fringe corresponds to a mirror movement of one half of the measurement wavelength, namely 410 nm. The amplitudes of the detector current signals, $(I_0 \cdot V/2)$, were 0.5 and 0.4 nA, with optical crosstalk signals of 35 and 16 nA, respectively. Due to thermal fluctuations on the chip, a noise current with an amplitude of about 20 pA was seen in the detector current, such that the signal noise corresponded to about 5% of the output signal amplitude.

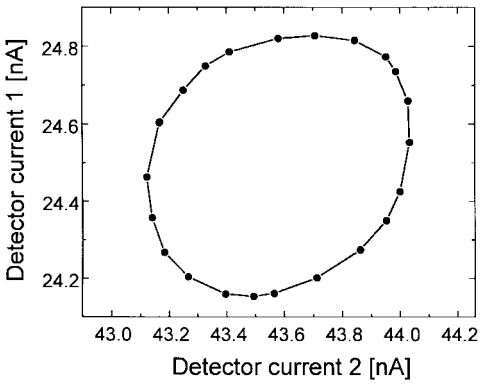

Fig. 9. The two detector currents of the double Michelson interferometer for 3.5 cm mirror distance and 67% mirror reflectance plotted as a function of each other; the signal rotates around the figure at a rate of 1.1 nm/°.

Plotting the two interferometer detector currents against each other resulted in the elliptical Lissajous-figure shown in Fig. 9. The ratio of the two normalized ellipse main axes allowed an estimate of the phase shift between the two reference signals, between 75–80°. Since one rotation (360°) of the characteristic corresponds to a mirror movement of 410 nm, we obtain a system measurement resolution of approximately 1.1 nm/°. If, based on the noise magnitude mentioned above, we conservatively estimate the angular interpolation to be limited to $2\pi/20$, or 18°, an interferometer displacement resolution of 20 nm is easily achieved. A further improvement of the resolution can be achieved by using an exactly circular Lissajous characteristic; this requires a 90° phase shift between the two interference signals, achievable with a slightly longer phase shifter.

The slightly distorted sine- and cosine-shape of the two signals results from the parasitic reflection at the right cleaved facet of the sensing beam. This reflection at the measurement facet and the reflection at the object mirror generate a Fabry–Pérot interferometer cavity, whose electric field interferes with the one from the reference arm. We studied the behavior of such a three-mirror interferometer by simulation and were able to predict the asymmetric shape of the interferograms when changing the intrinsic phase between reference and sensing arm, as seen experimentally and in agreement with a similar, more comprehensive study in the literature [29].

The maximum measurement distance for the DMI was 25 cm, corresponding to a laser linewidth of about 1 GHz. In addition to optical feedback into the laser, the modal behavior of the sensing beam waveguide was not ideal; higher order waveguide modes could be observed under different coupling conditions. This effect further reduced the contrast and gave rise to occasional "mode hopping," which was clearly indicated by spontaneous changes of the phase between the two interferometer signals.

VII. Conclusions

Monolithically integrated single Michelson interferometers and double Michelson interferometers for contactless optical displacement measurement and direction determination have been demonstrated. The devices consisted of a DBR laser, detectors, modulators, and waveguides, all fabricated on a single GaAs/AlGaAs-chip. Displacement measurements were performed using only one external element for beam collimation and a movable mirror as measurement object.

The monolithic double Michelson interferometer was demonstrated to have a displacement resolution of 20 nm for measurement distances of up to 5 cm. In comparison, 250 nm displacement resolution at distances of 25 cm have been reported for nonmonolithic integrated optical implementations [7], [9] and 1 nm resolution, at a distance of several centimeters, has been reported [8] for a glass-based double interferometer. A 100 nm resolution for short distances has also been demonstrated for a monolithic interferometer [12], but without phase-shift between the measurement signals.

Concerning design improvements, we expect a considerable crosstalk reduction by etching an isolation trench with a depth of at least 800 nm and subsequent p-metal coating of the trench sidewalls. Furthermore, a maximized laser output power and a symmetric splitting ratio of the directional couplers will result in larger detector signals without increasing feedback of light into the laser cavity. Finally, AR-coated facets may reduce feedback and help to enlarge the coherence length of the laser.

Possible applications for this device are short range displacement measurements in microsystems, in order to monitor the deflection of an AFM cantilever or the movement of a diaphragm. A further interesting area of application is displacement measurement at longer distances, for example in height gauges or in precision machine tools. For both of the above applications, a wavelength stabilization of 10^{-6}, achieved by locking the laser frequency on a Cs or Rb absorption line, would be necessary.

Acknowledgment

The authors are grateful to J. E. Epler and H. P. Schweizer for crystal growth; P. Riel, D. Jeggle, and A. Vonlanthen for processing assistance; Y. Salvadé for laser linewidth measurements; J. Söchtig for valuable discussions; and M. T. Gale and H. W. Lehmann for their generous support.

References

[1] A. A. Michelson, "The relative motion of the earth and the luminiferous ether," *Amer. J. Sci.*, vol. 22, pp. 120–129, 1881.

[2] ———, "On the application of interference methods to spectroscopic measurements," *Phil. Mag.*, vol. 34, pp. 280–299, 1892.

[3] M. Born and E. Wolf, "Interference and interferometers," *Principles of Optics*, 6th ed. New York: Pergamon, 1984, pp. 256–323.

[4] F. T. Arecchi and A. Sona, "Long distance interferometry with a He–Ne-laser," *J. Appl. Phys. Math.*, vol. 16, pp. 128–129, 1965.

[5] H. P. Zappe, H. E. G. Arnot, and R. E. Kunz, "Technology for III–V-based integrated optical sensors," *Sensors Mat.*, vol. 6, pp. 261–270, 1994.

[6] D. Hofstetter, H. P. Zappe, and R. Dandliker, "Monolithically integrated optical displacement sensor in GaAs/AIGaAs," *Electron. Lett.*, vol. 31, pp. 2121–2122, 1996.

[7] ———, "A monolithically integrated double Michelson interferometer for optical displacement measurement with direction determination," *IEEE Photon. Technol. Lett.*, vol. 8, pp. 1370–1372, Oct. 1996.

[8] G. Ulbers, "An integrated optics sensor on silicon for the measurement of displacement, force and refractive index," *Proc. SPIE*, vol. 1506 "Micro-Optics II," pp. 99–110, 1991.

[9] Hommelwerke Sensor GmbH, Laser Interferometer HC250.

[10] D. Jestel, A. Baus, and E. Voges, "Integrated-optic interferometric microdisplacement sensor in glass with thermo-optic phase modulation," *Electron. Lett.*, vol. 26, pp. 1144–1145, 1990.

[11] G. Voirin, L. Falco, O. Boillat, O. Zogmal, P. Regnault, and O. Parriaux, "Monolithic double interferometer displacement sensor with wavelength stabilization," in *Proc. Euro. Conf. Integr. Opt. 93*, 1993, pp.12-28–12-29.

[12] T. Suhara, T. Taniguchi, M. Uemukai, H. Nishihara, T. Hirata, S. Iio, and M. Suehiro, "Monolithic integrated-optic position/displacement sensor using waveguide gratings and QW-DFB laser," *IEEE Photon. Technol. Lett.* vol. 7, pp. 1195–1197, 1995.

[13] S. Ura, T. Suhara, and H. Nishihara, "Integrated-optic interferometer position sensor," *J. Lightwave Technol.*, vol. 7, pp. 270–273, 1989.

[14] K. Yamaguchi, K. Okamoto, and T. Imai, "Selective area growth of GaAs by metalorganic chemical vapor deposition," *Japan J. Appl. Phys.*, vol. 24, pp. 1666–1671, 1985.

[15] D. Trommer, "Photonic integration on InP," in *Proc. ECIO'95*, Delft, The Netherlands, 1995, pp. 93–98.

[16] R. M. Larnmert, T. M. Cockerill, D. V. Forbes, and J. J. Coleman, "Dual-channel strained-layer InGaAs/GaAs/AlGaAs WDM source with integrated coupler by selective-area MOCVD," *IEEE Photon. Technol. Lett.*, vol. 6, pp. 1167–1169, 1994.

[17] D. Remiens, B. Rose, M. Carre, and V. Hornung, "GaInAsP/InP integrated ridge laser with a butt-joined transparent optical waveguide fabricated by single-step metalorganic vapor-phase epitaxy," *J. Appl. Phys.*, vol. 68, pp. 2450–2453, 1990.

[18] V. Hornung, D. Remiens, D. Robein, A. Gloukhian, and M. Carre, "Simple approach for monolithic integration of DFB laser and passive waveguide," *Electron. Lett.*, vol. 27, pp. 1683–1685, 1990.

[19] K. Meehan, P. Gavrilovic, N. Holonyak, Jr., R. D. Burnham, and R. L. Thornton, "Stripe-geometry Al_xGa_xAs quantum well heterostructure lasers defined by Si diffusion and disordering," *Appl. Phys. Lett.*, vol. 46, pp. 75–77, 1985.

[20] R. L. Thornton, J. E. Epler, and T. L. Paoli, "Monolithic integration of a transparent dielectric waveguide into an active laser cavity by impurity-induced disordering," *Appl. Phys. Lett.*, vol. 51, pp. 1983–1985, 1987.

[21] J. Beauvais, S. G. Ayling, and J. H. Marsh, "Low-loss extended cavity lasers by dielectric cap disordering with a novel masking technique," *IEEE Photon. Technol. Lett.*, vol. 4, pp. 372–373, 1993.

[22] D. Hofstetter, H. P. Zappe, J. E. Epler, and P. Riel, "Multiple wavelength Fabry–Pérot lasers fabricated by vacancy-enhanced quantum well disordering," *Appl. Phys. Lett.*, vol. 67, pp. 1978–1980, 1995.

[23] R. J. Deri, W. Doldissen, R. J. Hawkins, R. Bhat, J. B. D. Soole, L. M. Schiavone, M. Seto, N. Andreadakis, Y. Silberberg, and M. A. Koza, "Efficient vertical coupling of photodiodes to InGaAsP rib waveguides," *Appl. Phys. Lett.*, vol. 58, pp. 2749–2751, 1991.

[24] K.-Y. Liou, U. Koren, E. C. Burrows, M. Oron, B. J. Miller, M. Young, G. Raybon, and C. A. Burrus, "Operation of integrated InGaAsP/InP optical amplifier-monitoring detector with feedback control circuit," *IEEE Photon. Technol. Lett.*, vol. 2, pp. 878–880, 1990.

[25] P. Vettinger, M. K. Benedict, G.-L. Bona, P. Buchmann, E. C. Cahoon, K. Dätwyler, H.-P. Dietrich, A. Moser, H. K. Seitz, O. Voegeli, D. J. Webb, and P. Wolf, "Full-wafer technology—A new approach to large-scale laser fabrication and integration," *IEEE Quantum Electron.*, vol. 27, pp. 1319–1331, 1991.

[26] C.-H. Chen and S.-C. Lee, "Monolithic integration of an AlGaAs/GaAs surface emitting laser diode and a photodetector," *Appl. Phys. Lett.*, vol. 59, pp. 3592–3594, 1991.

[27] D. Hofstetter, H. P. Zappe, J. E. Epler, and J. Sochtig, "Single-growth-step GaAs/AIGaAs distributed Bragg reflector lasers with holographically-defined recessed gratings," *Electron. Lett.*, vol. 30, pp. 1858–1859, 1994.

[28] D. Hofstetter, H. P. Zappe, and J. E. Epler, "Ridge waveguide DBR lasers with nonabsorbing grating and transparent integrated waveguide," *Electron. Lett.*, vol. 31, pp. 980–982, 1995.

[29] W. E. Ward, Z. Pasturczyk, W. A. Gault, and G. G. Shepherd, "Multiple reflections in a wide-angle Michelson interferometer," *Appl. Opt.*, vol. 24, pp. 1589–1598, 1985.

Daniel Hofstetter was born in Zug, Switzerland, in 1966. He received the Dipl. Phys. ETH degree in physics from the Swiss Federal Institute of Technology in 1993. His diploma thesis entitled "CO-Laser Photoacoustic Spectroscopy of Fatty Acid Vapors," was carried out under the supervision of Prof. F. K. Kneubühl at the Infrared Physics Laboratory of the ETH in Zurich. He received the Ph.D. degree in physics from the Paul Scherrer Institute in Zurich, in 1996, for his dissertation entitled "Monolithically Integrated Interferometer for Optical Displacement Measurement."

After an apprenticeship at Landis & Gyr in Zug as an electrical mechanic from 1982 to 1986, he worked for the same company as a Physics Technician. He is currently involved in InGaN blue laser diode research at the Xerox Palo Alto Research Center in Palo Alto, CA.

Hans P. Zappe was born in Paris, France, in 1961. He received the B.S. and M.S. degrees in electrical engineering from the Massachusetts Institute of Technology (M.I.T.), Cambridge, in 1983 and the Ph.D. degree in electrical engineering from the University of California, Berkeley, in 1989.

He has worked for IBM in Essex Junction, VT, and the Fraunhofer Institute for Applied Solid State Physics in Freiburg, Germany, at first on silicon VLSI and subsequently on III–V optics. He is presently at the Paul Scherrer Institute in Zurich, Switzerland, leading projects on the development of photonic integrated circuits and custom semiconductor lasers for sensor and metrology applications, and teaches integrated optics at the Neu-Technikum in Buchs, Switzerland.

René Dändliker was born in Zug, Switzerland, in 1939. He received the Diploma in physics from the Swiss Federal Institute of Technology, Zurich, Switzerland, in 1963, the Ph.D. degree in physics from the University of Berne, Switzerland, in 1968, and the Venia Legendi for applied physics at the Swiss Federal Institute of Technology, Zurich, in 1978.

From 1963 to 1969, he was Graduate Research Assistant at the Institute of Applied Physics, University of Berne, where he worked on gas and solid-state lasers. From 1969 to 1970, he was Research Scientist at the Philips Research Laboratories, Eindhoven, The Netherlands, in the field of applied optics. From 1970 to 1978, he was Senior Scientist and Head of the Coherent Optics Group at the Brown Boveri Research Center, Baden, Switzerland, where he was concerned with optical metrology applied to mechanics, such as laser Doppler velocimetry and heterodyne holographic interferometry. Since 1978 he has been Professor of Applied Optics at the University of Neuchatel, Switzerland, and since 1989, he has also been a Professor of applied optics at the Swiss Federal Institute of Technology, Lausanne. His current research activities are in optical metrology, optical fibers and sensors, holography and optical computing, diffractive optical elements, and micro-optics.

Dr. Dändliker is Past-President of the European Optical Society (EOS), a Vice-President of the International Commission for Optics (ICO), a fellow of the OSA, the Swiss Academy of Engineering Sciences (SATW), member of the SPIE, the French Society of Optics (SFO), the German Society of Applied Optics (DGaO), the European Physical Society (EPS), and an affiliate member of LEOS/IEEE.